# Supporting information

## A Systematic Effect for an Ultra-long Cycle Lithium-sulfur Battery

*Feng Wu,*[†,‡,⊥] *Yusheng Ye,*[†,⊥] *Renjie Chen,*[*,†,‡] *Ji Qian,*[†] *Teng Zhao,*[†] *Li Li,*[†,‡] *Wenhui*[†]

† Beijing Key Laboratory of Environmental Science and Engineering, School of Material Science & Engineering, Beijing Institute of Technology, Beijing 100081, China

‡ Collaborative Innovation Center of Electric Vehicles in Beijing, Beijing 100081, China.

∗Corresponding author at: Beijing Key Laboratory of Environmental Science and Engineering, School of Materials Science and Engineering, Beijing Institute of Technology, Beijing 100081, China. Tel.: +86 10 68912508; fax: +86 10 68451429.

E-mail addresses: chenrj@bit.edu.cn (R. Chen).

[⊥] These authors contributed equally to this work.

## Experimental section

**Synthesis of HCNTs:** 2.0 g aligned carbon nanotubes (Shenzhen Nanotech Port Co., China; specific surface area 185.73 $m^2$ $g^{-1}$, diameter 10-20 nm, length 5-15 mm) were dispersed in 6.4 g NaOH (Alfa Aesar) aqueous solution (80 mL, 2 M) with ultra-sonication for 30 min at room temperature. The mixture was transferred into a stainless steel reaction autoclave (100 mL) and heated to 180°C. After 3 h reaction, the reacted mixture was cooled to room temperature. The reaction mixture was washed with methanol, ethanol and deionized water until the pH reached 7.0 and dried in a vacuum oven at 60°C to yield HCNTs.

**Synthesis of S-HCNTs nanocomposite:** 0.08 mol $Na_2S_2O_3$ (J&K, AR) and as-synthesized HCNTs (2 g) were dissolved in deionized water (2 L), followed by strong mechanical stirring for 30 mins. After another 30mins ultra-sonication and the suspension were well dispersed, 80 mL dilute hydrochloric acid (0.2 mol/L, J&K) was added into the solution dropwise by peristaltic pump (20 μL/min) under ultra-sonication in a draught cupboard at 20°C to precipitate sulfur homogeneously on the HCNTs. The reaction proceeded 12h and after that the product was centrifuged, washed with deionized water, and dried under vacuum at 60°C for 48h.

**Synthesis of PD-S-HCNTs:** The dried S-HCNTs (2 g) were dispersed in Tris-HCl (pH 8.5, 2 L) solution under stirring. Dopamine (0.5 g/L, Alfa Aesar, 98%) solution was added dropwise by peristaltic pump (0.4 mL/min) in a draught cupboard to polymer PD on the S-HCNTs homogeneously, with ultra-sonication and at 20°C. Polymerization was maintained for 4 h to form a PD coated S-HCNTs composite. Then the PD coated S-HCNTs composite was collected by centrifugation at 5000 rpm, washed with water three times and dried in an oven at 60°C for further use.

**Synthesis of PD-treated separator:** The synthesis of PD treated separator was based on a modified PD in-situ coating process[1]. The PE separators were immersed into the dopamine solution (10 mM) with methanol and Tris-buffered solution (pH 8.5) as co-solvents ($CH_3OH$: Tris-HCl = 1:1 by volume). The same procedure as for the synthesis of the other side was applied to obtain a bilaterally modified separator. After 24 h of soaking, the separators were removed, rinsed with deionized water and dried under argon.

**Material characterization.** Fourier transform infrared spectra are recorded using a Nicolet iS10 spectrometer (Thermo, USA) from 4000 to 500 $cm^{-1}$ with a resolution of 4 $cm^{-1}$. Raman

spectra are measured on a Raman spectrometer (Renishaw-1000) with an excitation laser beam wavelength of 532 nm. X-ray diffraction measurements are performed using a diffractometer (Rigaku) with a Cu Kα radiation source (λ=0.154 nm). The morphology of the composites is determined by field-emission scanning electron microscopy (SUPRA 55 and FEI Quanta 250) and high-resolution transmission electron microscopy (JEOL-2010 and TECNAI G2 20, 200 kV). Thermal gravimetric analysis (TGA) is carried out using a thermal analyzer (6200 EXSTAR) at a heating rate of 10 °C/min under an air atmosphere. The morphology and composition of the surfaces of the anode/cathode surface are investigated with EDX and SEM (HTACHI S-4800) under argon protection condition.

**Electrochemical Measurements.** CNTs-S, S-HCNTs and PD-S-HCNTs composite cathode slurries are produced by mixing 70% composite, 20% carbon black, and 10% polyvinylidene fluoride (PVDF) binder in N-methyl-2-pyrrolidinone (NMP). The mixtures are ball milled for 6h to form homogeneous slurries. After stirring, each slurry is coated onto aluminum foil. The coated electrodes are dried in a vacuum oven at 60 °C for 48 h. The sulfur loading of the as-obtained electrode is around 1.7~1.8 mg/cm$^2$. The electrodes are cut into disks with a diameter of 11 mm. Two-electrode coin cells (CR2032) with Li foil as the counter electrode are assembled in an argon-filled glove box for electrochemical experiments. The electrolyte used is 1.0 M bis-(trifluoromethane)sulfonimide lithium (LiTFSI) and 0.2M $LiNO_3$ in a 1:1 v/v mixture of 1,2-dimethoxyethane (DME) and 1,3-dioxolane (DOL). The cells are discharged and charged from 1.7–3.0V at different current densities of S using an electrochemical station (LAND, Wuhan) to test their cycle life. Cyclic voltammograms are recorded on an electrochemical workstation (CHI660D, Shanghai Chenhua) between 1.7 and 3.0 V to characterize the redox behavior and kinetic reversibility of the cells. AC impedance is also measured using the CHI660D electrochemical workstation. The AC amplitude is ±5 mV, and the applied frequency range is from 100 kHz to 0.01 Hz.

**Material calculation.** The simulations are carried out using molecular simulation software for materials science, Materials Studio version 5.5, designed by Accelrys, Inc. Geometry optimizations of the radicals are carried out with the all-electron density functional program DMol$^3$ using the Becke−Lee−Yang−Parr (BLYP) functional and the double numerical plus polarization (DNP) basis set. Annealing protocol simulation is used to further optimize the

membrane structure. The polymers are constructed in amorphous cell using COMPASS27 forcefield.

**Supplementary data**

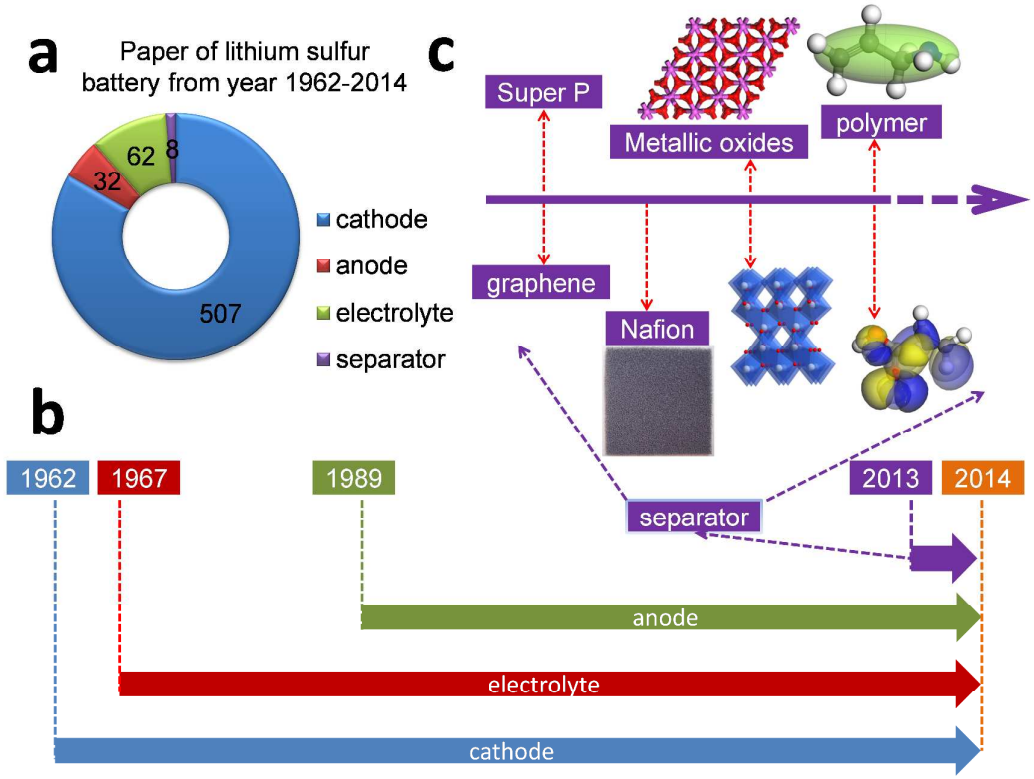


**Figure S1.** (a) Statistics of publication of lithium sulfur batteries from year 1962-2014. (b) Timelines of the advances in lithium sulfur batteries, covering cathode, electrolyte, anode and separator. (c) Recent advances in separator of lithium sulfur batteries. Data were collected from the "Web of Science".

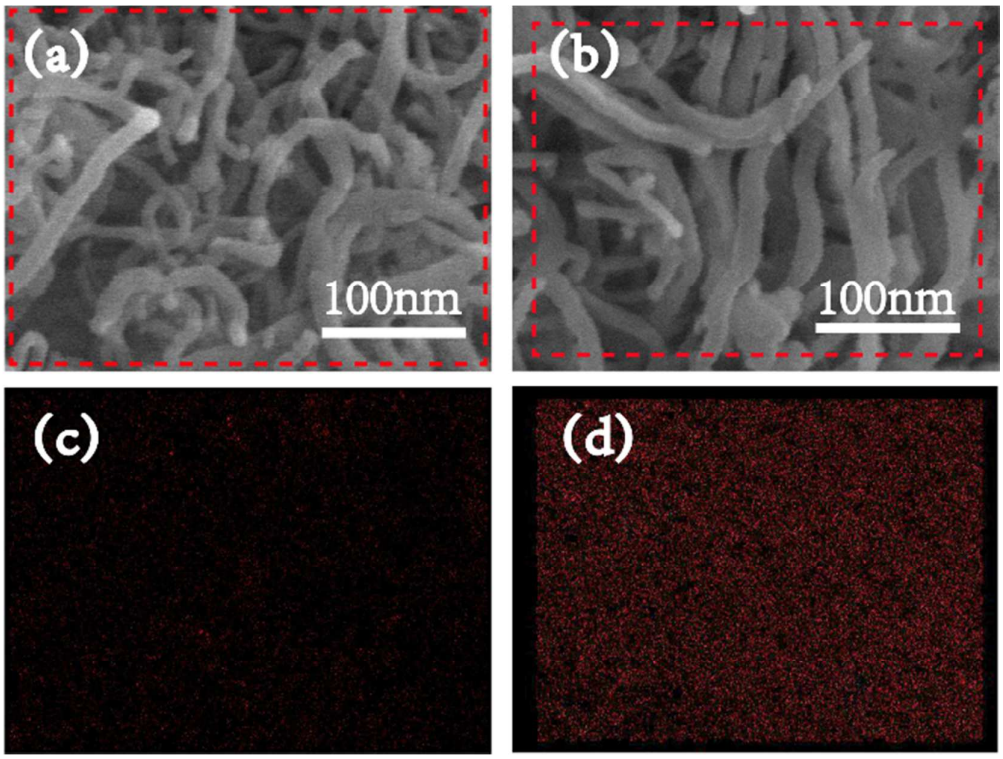


**Figure S2.** SEM images of CNTs (a) and HCNTs (b) materials, corresponding oxygen elemental mapping profiles of CNTs (c) and HCNTs (d). The mappings were conducted with same conduction and same scan cycles (12 cycles).

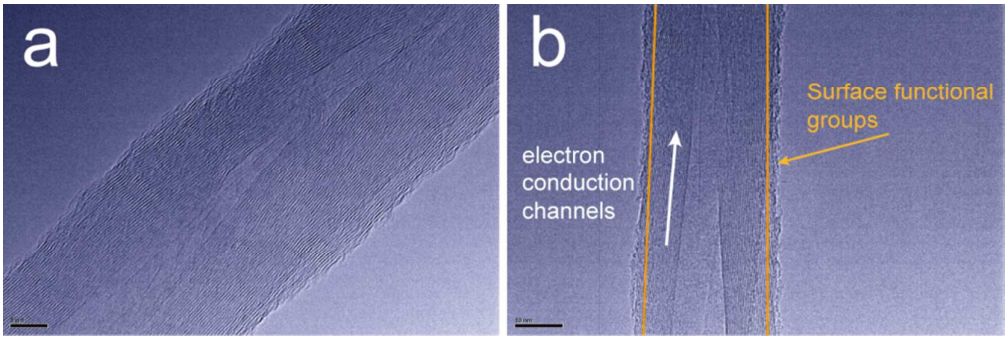


**Figure S3.** TEM images of CNTs (a) and HCNTs (b) material, corresponding surface oxygen functional species (orange arrow). Intact graphite layers inside the HCNTs (white arrow) are indicated as electron conduction channels.

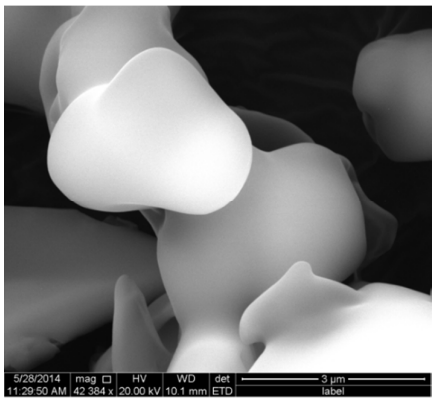

**Figure S4.** SEM image of sulfur clusters on HCNTs under high hydrochloric acid dropping speed (8 mL/min) condition and without ultra-sonication.

With high dropping speed and without ultra-sonication, the HCNTs structures are filled rapidly with the chemical active phase, the interconnection were closed partially during deposition, which prevent conformal deposition of the chemically active material onto the HCNTs surface. Thus, the ion pathway is not continuous. This phenomena eventually limits allowable charge and discharge rate. So controlled dropping speed and ultra-sonication is critical to form well-distributed cathode material.

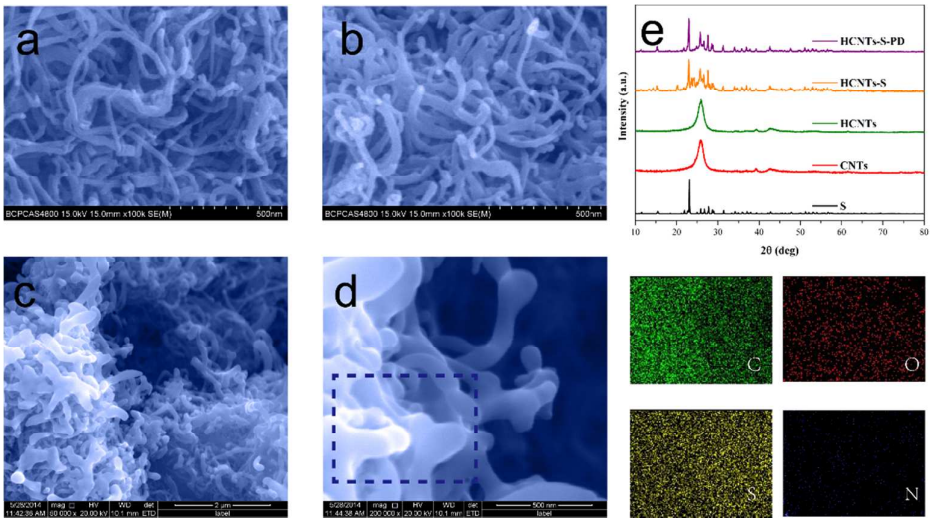


**Figure S5**. SEM images of (a) CNTs, (b) HCNTs, (C) S-HCNTs and (d) PD-S-HCNTs materials, corresponding elemental mapping profiles of PD-S-HCNTs material. XRD pattern with sulfur and the four mentioned materials above. (e) XRD patterns of S, CNTs, HCNTs, HCNTs-S and HCNTs-S-PD materials.

**Figure S5** presents scanning electron microscopy images of the synthesized materials, and demonstrates that sulfur is coated onto the HCNTs. The diameter of CNT and HCNTs are about 10~50nm, the continuous and aligned CNTs structure provides mechanical and electrical interconnections throughout the network. The diameter of S-HCNTs is about 40~100nm. To achieve a more stable cathode, the PD membrane is polymerized in a Tris-HCl buffer solution (pH 8.5) onto the above composite, with a diameter of about 50~120nm. This bifunctional interface architecture, which consists of active material located between a thin PD layer and HCNTs conductive scaffold phases, provides a highly conductive pathway for electrons, a short ion diffusion length in the intercalation compound and a fast mass transport channel in the liquid electrolyte.

The PD-S-HCNTs composite exhibits similar X-ray diffractometry (XRD) characteristic peak patterns to sulfur with an Fddd orthorhombic structure **(Figure S5e)**, which is overlapped with that of sulfur at 2θ = 23.0°, 26.6° and 27.6°. XRD results confirm that sulfur in the S-HCNTs-PD composite is highly crystalline and maintains the same crystal structure as $S_8$.

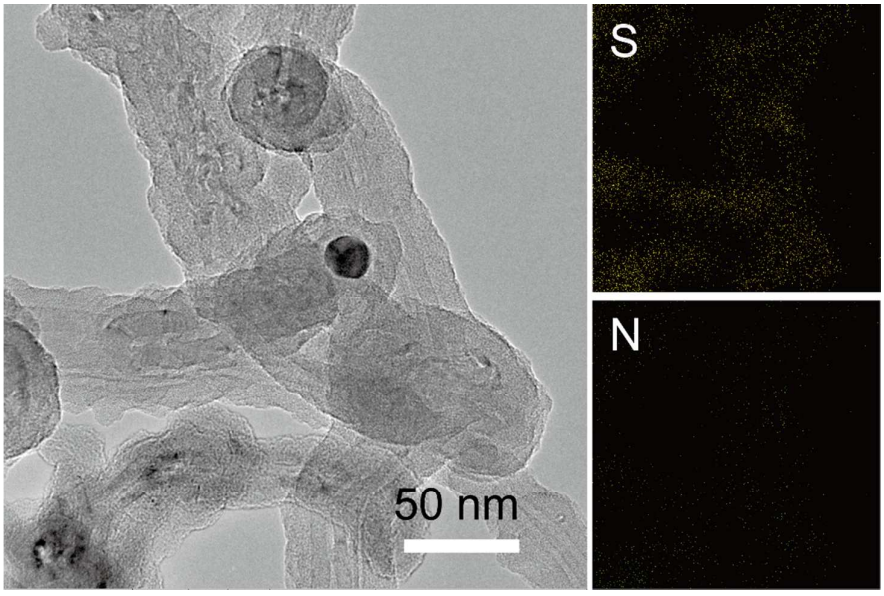


**Figure S6.** TEM image of PD-S-HCNTs, its corresponding sulfur and nitrogen elemental mapping profiles are also shown. Nitrogen elemental mapping represent the PD distribution in the composite surface.

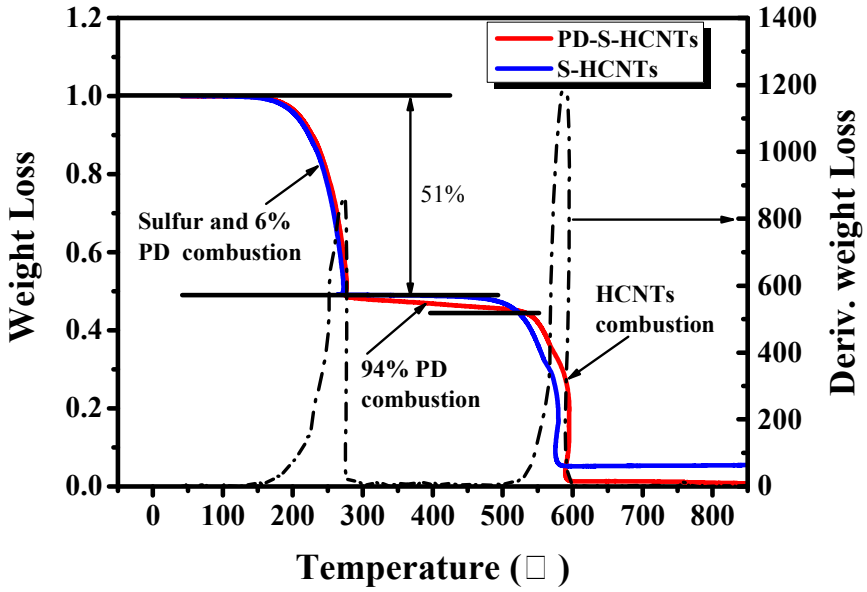


**Figure S7.** Thermogravimetric analysis (TG) curves of (a) S-HCNTs and (b) PD-S-HCNTs.

It is calculated that the weight percentage of S is 51 wt% and HCNTs is 49 wt% in the S-HCNTs composite. The weight loss of pure PD between 150 and 270 °C is about 6wt% only.[2] As the red curve shows, the weight loss between 150 and 270 °C is about 51 wt%, due to the oxidation of S and 6% PD combustion. So, the weight percentage of S, PD, and HCNTs are 50.8, 4.3, and 44.9 wt% in the PD-S-HCNTs composite, respectively.

In order to achieve high rate performance in our lithium sulfur system, conductivity is critical for cell. Thus, we increase the amount of HCNTs to increase conductivity. Even though the sulfur content in our PD-S-HCNTs is 50.8%, however, the thickness of our cathode can be achieve as high as 60 μm due to the excellent wettability and hydrophilic of PD, which significantly increases the uptake speed of electrolyte. Thus, the sulfur loading of the as-obtained electrode can be as high as 1.7~1.8 mg/cm$^2$.

**Figure S8.** Contact angle compared between PE bare separator and PD modified separator by adding 0.04ml electrolyte.

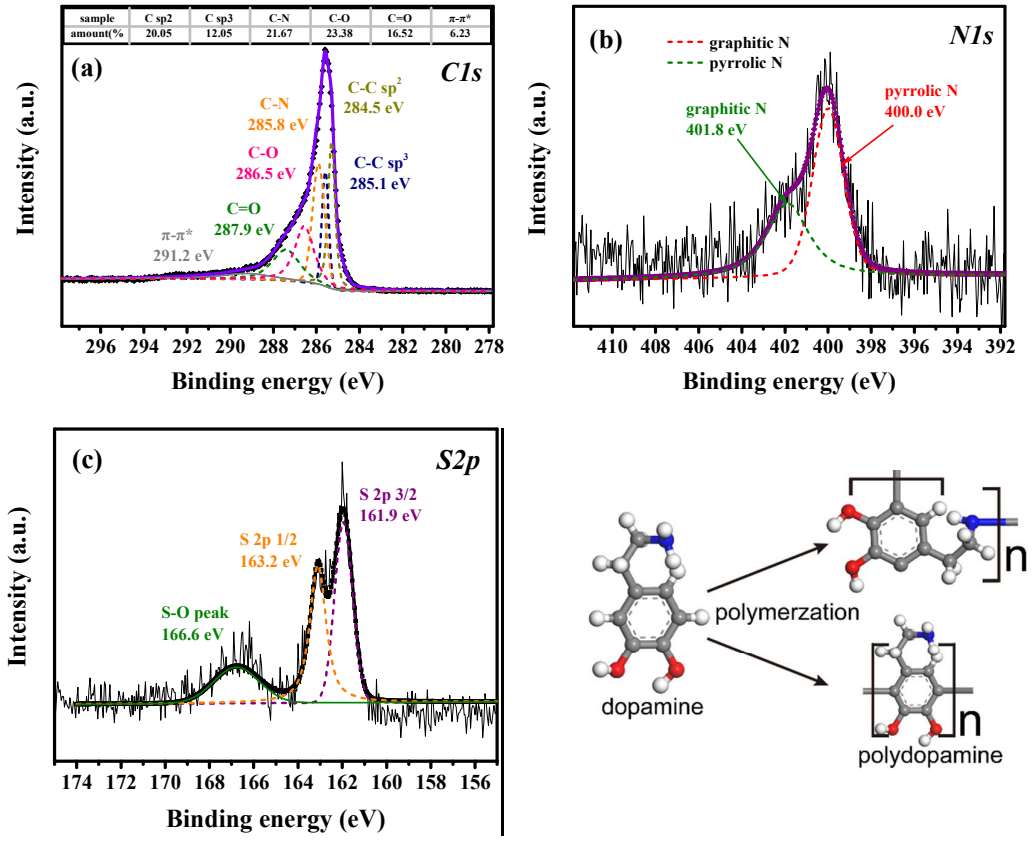


**Figure S9.** The high resolution C1s (a), N1s (b) and S2p (c) XPS spectrum are also shown to investigate the polymerization of PD in our cathode. The N1s XPS spectrum of PD-S-HCNTs/PD modified separator can be deconvoluted into two different signals with binding energies of 400.0, and 401.8 eV, corresponding to pyrrolic N and graphitic N, which confirm that the polymerization of dopamine conducts as illustrator in **Figure S9**. Furthermore, a sharp C 1s XPS peak at 286.5 eV is detected, indicating a domination of C-OH bonding in the materials. As for conventional C-S materials, the contents of C-OH located at 286.5 eV are much lower[3, 4], indicating the PD-S-HCNTs material is full of C-OH group, which plays one of key role roles in trapping sulfides.

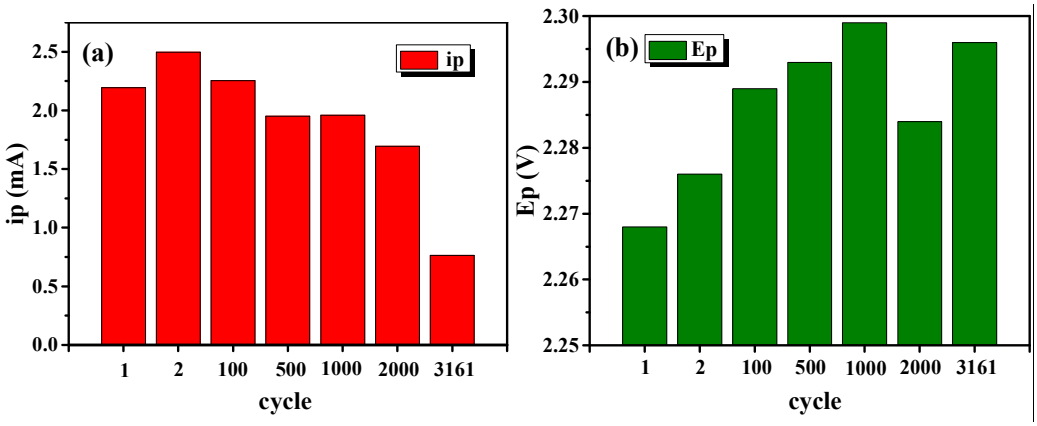


**Figure S10.** CV profile information of the PD-S-HCNTs/PD modified separator coin cell. Statistical analysis of oxidational $i_P$ (a) and $E_p$ (b) after different cycles, corresponding with **Figure 3a.**

To understand the electrochemical behavior of our systematic modified PD-S-HCNTs/PD cell, we analyzed the relationship between peak current-voltage and cycles. Thick cathode leads to an increased CV peak current ($i_P$) in the second cycle **(Figure S10a)** due to deeper soak of electrolyte. After fully soaked, the CV profiles decrease cathodic and anodic peaks only slightly in the first 2000 cycles, which prove that sulfur dissolution into electrolyte is effectively suppressed, thereby resulting in an effective capacity retention. Changes in charge peak voltage ($E_p$) are consistent with changes in $i_P$, charge peak voltage only decreases from 2.299 V to 2.284 V on the 2000th cycle **(Figure S10b)** due to inevitable dissolution of polysulfides.

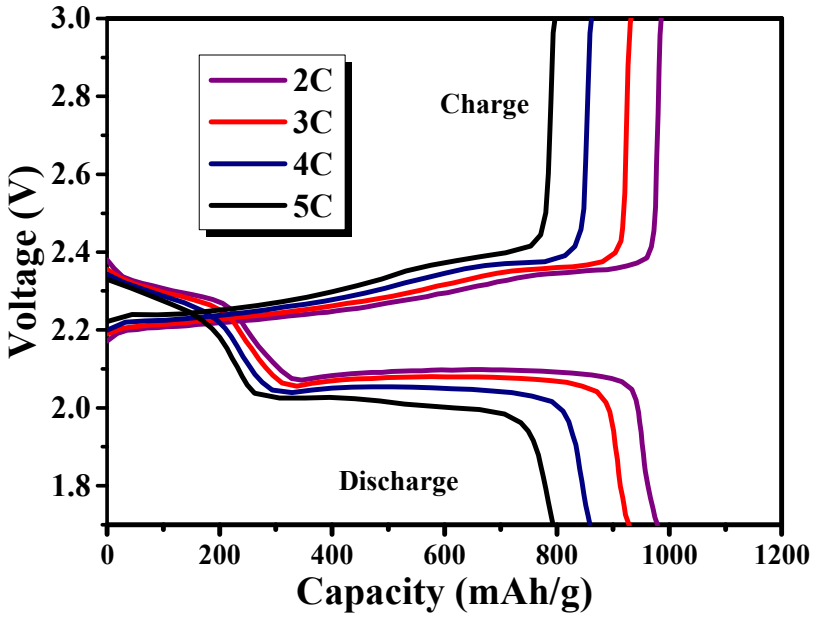


**Figure S11.** Galvanostatic charge/discharge profiles of the PD-S-HCNTs/PD coin cell at various rates from 2C to 5C, corresponding with **Figure 4d**. All discharge and charge curves contain two plateaus that correspond to the peaks in CV profiles.

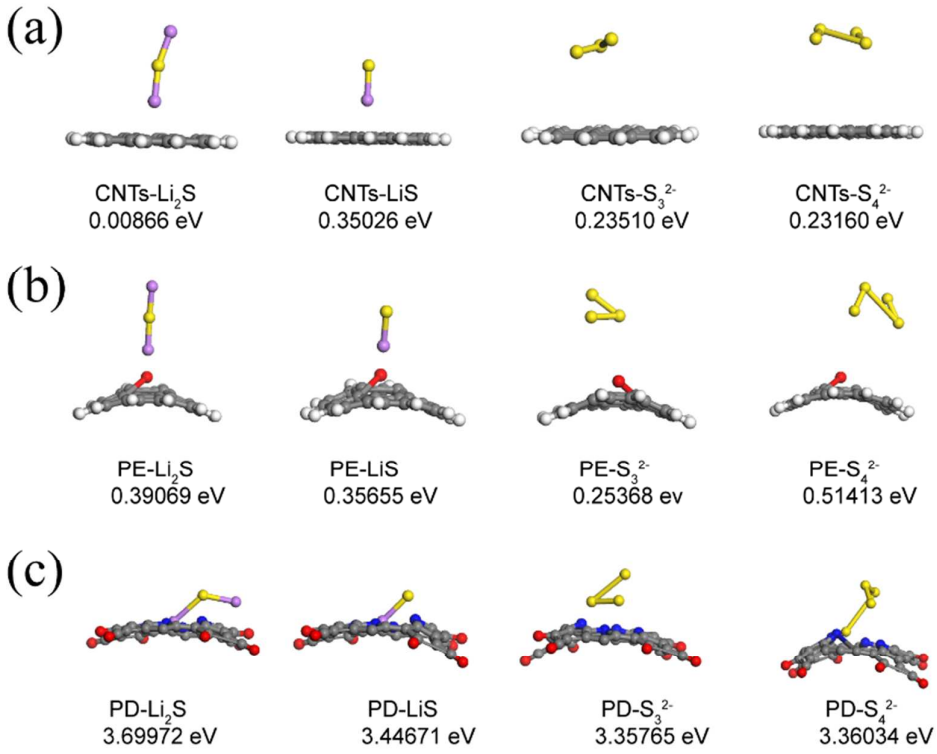


**Figure S12.** The side view of $Li_2S$, LiS, $S_3^{2-}$, $S_4^{2-}$ on CNTs (a), HCNTs (b), and PD (c) surfaces, which corresponding with **Figure 4**. S, C, O, and H atoms are represented by yellow, dark gray, red, and white balls. The calculated charge binding energy are also shown.

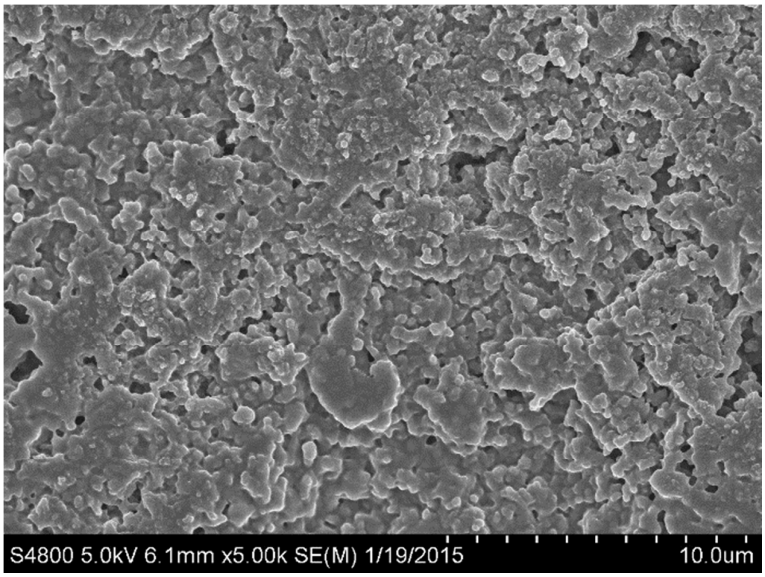


**Figure S13.** Surface morphology of the HCNTs-S-PD cathode cycled with the PD modified separator at 2C after 3000 cycles (at completed charged state).

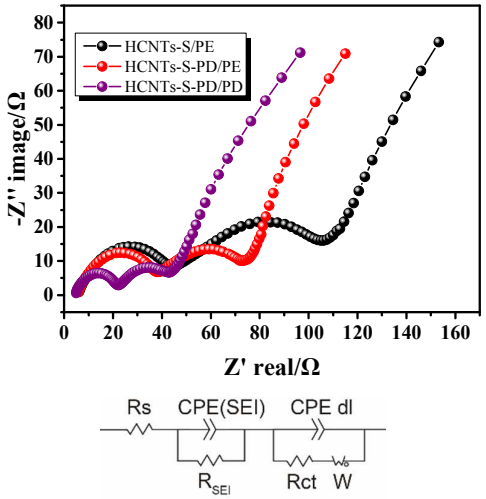


**Figure S14** Nyquist plots of the coins in different configurations recorded after cycled 11 cycles at 2C and their corresponding equivalent circuit model.

It is a typical model for analyzing Nyquist plot consisting of two semicircle at high frequencies and an inclined line in the low frequency region. There are five parameters in the model: Rs, Rct, $R_{SEI}$, W and CPE. Among them, Rs and Rct are relate to electrochemical activities of the composites. Rs is the impedance contributed by the resistance of the electrolyte while Rct is the charge transfer resistance at the interface between the electrode and electrolyte. In addition, $R_{SEI}$ is the impedance contributed by (solid electrolyte interface) SEI film. Moreover, W represents a

semi-infinite Warburg diffusion process of soluble lithium polysulfide in the electrolyte. Specially, the constant-phase element (CPE) here describes the double layer capacitance distributed on the surface of the carbon.

The $R_{SEI}$ of HCNTs-S/PE, PD-S-HCNTs/PE and PD-S-HCNTs/PD are 41.3 Ω, 36.7 Ω, and 16.0 Ω. In the HCNTs-S/PE system, the main component of SEI is $Li_2S$, which is a poor lithium ion conductor. With PD protection, the dissolution polysulfides is alleviated and the composition of SEI layer is different, which lead to a significantly $R_{SEI}$ decrease than HCNTs-S/PE system's. Thus, PD treated cells form more stable SEI layers and facilitate more effective Li-ion transfer at the interfaces.

Moreover, the value of interfacial resistance Rct for the PD-S-HCNTs/PD separator system (28.0 Ω) is lower than that of the PD-S-HCNTs/PE (36.7 Ω) and the HCNTs-S/PE system (70.4 Ω) because of due to enhanced hydrophilicity improves the electrolyte uptake speed and helps to increase the ionic conductivity. This thin PD layer therefore decreases charge transfer compared with others, because charge transfer is directly associated with the migration of Li ions at the electrode-electrolyte inter-faces.

**Table S1** The performance of different structure first introduced into lithium sulfur battery and their further typical performance.

| Researches | | Since | C-rate | Cycles | Dis. Capa. | S content | Typical[Dis./C/R/CR] | Ref. |
|---|---|---|---|---|---|---|---|---|
| **Cathode** | | | | | | | | |
| Core-shell | | 2011 | 100mA/g | 80 | 932.4 | 70.0 wt% | 380/200/10C/0.019% | R[5, 6] |
| Yolk-shell | | 2013 | 0.5C | 1000 | 690 | 71.0 wt% | 780/500/0.5C/0.0122% | R[7, 8] |
| Carbon nanotube | | 2009 | 100mA/g | 60 | 670 | 68.0 wt% | 990/500/1C/0.00172% | R[9, 10] |
| 2D-3D graphene | | 2011 | 1C | 100 | 505 | 70.0 wt% | 353/2000/2C/0.028% | R[11, 12] |
| Porous | Microoporous | 2010 | 400mA/g | 500 | 650 | 42.0 wt% | 1149/200/0.1C/0.004% | R[13, 14] |
| | Mesoporous | 2009 | 0.1C | 20 | 1100 | 69.3 wt% | 830/100/1C/0.0017% | R[15, 16] |
| | Macroporous | 2011 | 0.5C | 100 | 974 | 70.0 wt% | 1223/150/0.5C/0.0024% | R[17, 18] |
| | Morphology | 2011 | 0.2C | 150 | 730 | 75.0 wt% | 680/300/0.92C/0.10% | R[19, 20] |
| **Anode** | | | | | | | | |
| Alloy | | 2013 | 0.2C | 50 | 580 | 80.0 wt% | — | R[21] |
| Membrane | | 2003 | 0.1C | 100 | 270 | 50.0 wt% | — | R[22, 23] |
| Hybrid anode | | 2014 | 1C | 400 | >800 | 50.0 wt% | — | R[24] |
| Li-Free | | 2014 | 1.28 mA/cm$^2$ | 200 | 800 | — | — | R[25] |
| **Electrolyte** | | | | | | | | |
| Solvent | | 1989 | 0.01 mA/cm$^2$ | — | — | — | 750/10/100 mAg$^{-1}$/— | R[26] |
| Liquid | | 2008 | 0.414 mA/cm$^2$ | 102 | 874 | 73.0 wt% | 770/100/0.2C/0.026% | R[27] |
| Gel | | 2000 | 0.1 mA/cm$^2$ | 20 | <100 | 50.0 wt% | 1050/100/0.2C/— | R[28, 29] |
| Solid | | 2003 | 64μA/cm$^2$ | 20 | 650 | — | 852/100/0.1C/0.0075% | R[30, 31] |
| **Battery structure system** | | | | | | | | |
| Graphene | | 2013 | 1.5 A/g | 300 | 680 | 70.0% | CD:0.1% per cycle | R[20] |
| Super P | | 2014 | 0.5C | 500 | 669 | <70.0% | CD:0.00836% per cycle | R[32] |
| Metallic oxide | | 2014 | unkown | 200 | 600 | 70.0% | CD:0.009% per cycle | R[33] |
| Polymer | | 2014 | unkown | 50 | about 400 | 50.0% | 522/500/3 A g$^{-1}$/0.064% | R[34, 35] |
| **Our work** | | **2014** | **2C** | **2000** | **636.8** | **50.8%** | **CD:0.015% per cycle** | |
| | | | **2C** | **3161** | **387.4** | **50.8%** | **CD:0.018% per cycle** | |

**Typical [Dis./C/R/CD] is the abbreviation of Typical [Discharge capacity/Cycles/Current rate/Capacity retention], which means the cell expresses _ discharge capacity (mAh/g) after _ cycles at _ current rate with a _ capacity retention.**

In a typical soft packaging lithium sulfur battery, active material is bilaterally coated on aluminum foil. Based on our work, the sulfur loading of the single-faced cathode is ~1.75 mg/cm$^2$. Thus, the sulfur loading of the double-faced cathode can be achieve as ~3.5 mg/cm$^2$. Additional, the sulfur content of the HCNTs-S-PD composite is 50.8 wt%, and the electrode film contains 70 wt% of the active composite material. So the mass of S cathode including binder and additive is around 9.9 mg/cm$^2$ (double face).

Here, we also calculate the specific energy (E) of designed cell in our work according to following equation:

$$E = \frac{QV_{avg}}{\sum M_i}$$

Where Q indicates the capacity and Vavg indicates the average voltage of Li/S cells.

$M_i$ is the sum of the weight of electrode component except cell-housing.

Table S2 shows values used for calculating specific energy considering a standard Li/S cell design. [36]

**Table S2. Values for estimation of the specific energy of different types of Li/S batteries**

| Design Parameters for Calculations of Cell Specific Energy Density | | | | |
|---|---|---|---|---|
| Cathode | | Electrolyte | | Anode |
| Al Foil | S electrode (including binder/additives) | Separator | Organic Solvent | Li Foil |
| 1.4 mg/cm$^2$ | 9.9 mg/cm$^2$ (double face) | 5 mg/cm$^2$ | | 3.6 mg/cm$^2$ |
| Total weight:19.9 mg/cm$^2$ | | | | |

The HCNTs-S-PD/PD-separator/Li cell delivers an initial discharge capacity of 1213 mAh/g, corresponding to 83% usage of S. Considering an average discharge voltage of 2V, the expected specific energy of HCNTs-S-PD/PD-separator/Li cell is ~439 Wh/kg. After the 100 cycles test at 0.2C, the discharge capacity still remains around 949 mAh/g, corresponding to the specific energy of ~343 Wh/kg, which is more than two times of that of common Li-ion battery (C/$LiCoO_2$, 160 Wh/kg). The HCNTs-S-PD/PD-separator/Li cell delivers a capacity of 631.5 mAh/g after 2000 cycles at 2C, corresponding to the expected specific energy of ~228 Wh/kg.

## Reference


1. Ryou, M. H.; Lee, D. J.; Lee, J. N.; Lee, Y. M.; Park, J. K.; Choi, J. W. *Adv. Energy Mater.* **2012**, 2, 645-650.
2. Wang, L.; Wang, D.; Zhang, F.; Jin, J. *Nano Lett.* **2013**, 13, 4206-4211.
3. Xie, Y.; Li, H.; Tang, C.; Li, S.; Li, J.; Lv, Y.; Wei, X.; Song, Y. *J. Mater. Chem. A*. **2014**, 2, 1631-1635.
4. Elazari, R.; Salitra, G.; Garsuch, A.; Panchenko, A.; Aurbach, D. *Adv. Mater.* **2011**, 23, 5641-5644.
5. Wu, F.; Chen, J.; Li, L.; Zhao, T.; Chen, R. *J. Phys. Chem. C.* **2011,** 115, 24411-24417.
6. Li, G. C.; Li, G. R.; Ye, S. H.; Gao, X. P. *Adv. Energy Mater.* **2012,** 2, 1238-1245.
7. Wei Seh, Z.; Li, W.; Cha, J. J.; Zheng, G.; Yang, Y.; McDowell, M. T.; Hsu, P. C.; Cui, Y. *Nat Commun.* **2013**, 4, 1331.
8. Li, W.; Zhang, Q.; Zheng, G.; Seh, Z. W.; Yao, H.; Cui, Y. *Nano Lett.* **2013**, 13, 5534-5540.
9. Yuan, L.; Yuan, H.; Qiu, X.; Chen, L.; Zhu, W. *J. Power Sources.* **2009,** 189, 1141-1146.
10. Chen, S.; Huang, X.; Liu, H.; Sun, B.; Yeoh, W.; Li, K.; Zhang, J.; Wang, G. *Adv. Energy Mater.* **2014**, 4, 1761..
11. Cao, Y.; Li, X.; Aksay, I. A.; Lemmon, J.; Nie, Z.; Yang, Z.; Liu, J. *Phys. Chem. Chem. Phys.* **2011**, 13, 7660-7665.
12. Qiu, Y.; Li, W.; Zhao, W.; Li, G.; Hou, Y.; Liu, M.; Zhou, L.; Ye, F.; Li, H.; Wei, Z.; Yang, S.; Duan, W.; Ye, Y.; Guo, J.; Zhang, Y. *Nano Lett.* **2014**, 14, 4821-4827.
13. Zhang, B.; Qin, X.; Li, G.; Gao, X. *Energy Environ. Sci.* **2010**, 3, 1531-1537.
14. Yin, Y. X.; Xin, S.; Guo, Y. G.; Wan, L. J. *Angew. Chem., Int. Ed.* **2013**, 52, 13186-13200.
15. Ji, X.; Lee, K. T.; Nazar, L. F. *Nat. Mater.* **2009**, 8, 500-506.
16. Schuster, J.; He, G.; Mandlmeier, B.; Yim, T.; Lee, K. T.; Bein, T.; Nazar, L. F. *Angew. Chem., Int. Ed.* **2012,** 51, 3591-3595.
17. Jayaprakash, N.; Shen, J.; Moganty, S. S.; Corona, A.; Archer, L. A. *Angew. Chem.* **2011**, 123, 6026-6030.
18. Moon, S.; Jung, Y. H.; Jung, W. K.; Jung, D. S.; Choi, J. W.; Kim, D. K. *Adv. Mater.* **2013**, 25, 6547-6553.
19. Zheng, G.; Yang, Y.; Cha, J. J.; Hong, S. S.; Cui, Y. *Nano Lett.* **2011**, 11, 4462-4467.
20. Zhou, G.; Pei, S.; Li, L.; Wang, D. W.; Wang, S.; Huang, K.; Yin, L. C.; Li, F.; Cheng, H. M. *Adv. Mater.* **2013**, 02, 625–631.
21. Duan, B.; Wang, W.; Zhao, H.; Wang, A.; Wang, M.; Yuan, K.; Yu, Z.; Yang, Y. *ECS Electrochem. Lett.,* **2013**, 2, A47-A51.
22. Lee, Y. M.; Choi, N.-S.; Park, J. H.; Park, J. K. *J. Power Sources.* **2003**, 119–121, 964-972.
23. Ding, F.; Xu, W.; Graff, G. L.; Zhang, J.; Sushko, M. L.; Chen, X.; Shao, Y.; Engelhard, M. H.; Nie, Z.; Xiao, J.; Liu, X.; Sushko, P. V.; Liu, J.; Zhang, J. G. *J. Am. Chem. Soc.* **2013**, 135, 4450-4456.
24. Huang, C.; Xiao, J.; Shao, Y.; Zheng, J.; Bennett, W. D.; Lu, D.; Saraf, L. V.; Engelhard, M.; Ji, L.; Zhang, J.; Li, X.; Graff, G. L.; Liu, J. *Nat. Commun.* **2014**, 5.
25. Hagen, M.; Quiroga-González, E.; Dörfler, S.; Fahrer, G.; Tübke, J.; Hoffmann, M. J.; Althues, H.; Speck, R.; Krampfert, M.; Kaskel, S.; Föll, H. *J. Power Sources.* **2014,** 248, 1058-1066.
26. Peled, E.; Sternberg, Y.; Gorenshtein, A.; Lavi, Y. *J. Electrochem. Soc.* **1989**, 136, 1621-1625.
27. Suo, L.; Hu, Y. S.; Li, H.; Armand, M.; Chen, L. *Nat. commun.* **2013**, 4, 1481.
28. Gao, J.; Lowe, M. A.; Kiya, Y.; Abruña, H. D. *J. Phys. Chem. C.* **2011**, 115, 25132-25137.

29. Mikhaylik, Y. V., Electrolytes for lithium sulfur cells. Google Patents: 2008.

30. Hayashi, A.; Ohtomo, T.; Mizuno, F.; Tadanaga, K.; Tatsumisago, M. *Electrochem. Commun.* **2003,** 5, 701-705.

31. Liu, Z.; Fu, W.; Payzant, E. A.; Yu, X.; Wu, Z.; Dudney, N. J.; Kiggans, J.; Hong, K.; Rondinone, A. J.; Liang, C. *J. Am. Chem. Soc.* **2013**, 135, 975-978.

32. Wei, H.; Ma, J.; Li, B.; Zuo, Y.; Xia, D. ACS Appl. Mater. Interfaces, **2014**, 6, 20276-20281.

33. Yao, H.; Yan, K.; Li, W.; Zheng, G.; Kong, D.; Seh, Z. W.; Narasimhan, V. K.; Liang, Z.; Cui, Y. *Energy Environ Sci* **2014,** 7, 3381-3390.

34. Zhou, G.; Li, L.; Wang, D. W.; Shan, X. y.; Pei, S.; Li, F.; Cheng, H. M. *Adv Mater.* **2014**, 27, 641-647.

35. Gu, M.; Lee, J.; Kim, Y.; Kim, J. S.; Jang, B. Y.; Lee, K. T.; Kim, B. S. *RSC Advances.* **2014,** 4, 46940-46946.

36. Cai, K.; Song, M. K.; Cairns, E. J.; Zhang, Y. Nano Lett. 2012, 12, 6474–6479.